Atmospheric Environment 210 (2019) 1–13

Contents lists available at ScienceDirect

Atmospheric Environment

journal homepage: www.elsevier.com/locate/atmosenv

Optimization of vertical grid setting for air quality modelling in China considering the effect of aerosol-boundary layer interaction

Zilin Wang[a,b], Xin Huang[a,b,*], Aijun Ding[a,b]

[a] Joint International Research Laboratory of Atmospheric and Earth System Sciences, School of Atmospheric Sciences, Nanjing University, Nanjing, 210023, China
[b] Jiangsu Provincal Collorative Innovation Center of Climate Change, Nanjing, 210023, China

ARTICLE INFO

Keywords:
Haze pollution
Aerosol-boundary layer interaction
Vertical grid setting
Air quality modelling

ABSTRACT

The feedback between ambient aerosols and planetary boundary layer (PBL) meteorology has been proven to play a critical role in the enhancement of haze pollution. Vertical distribution of aerosols as well as temperature stratification are vital to understand aerosol – boundary layer interaction (ABI) and its impact on air quality deterioration. In current regional air quality models, the default vertical grid setting is relatively coarse and decreases progressively with altitude. However, the ABI is sensitive to aerosol layer at specific altitudes, i.e. around the top of PBL. This work aims to explore optimized vertical grid setting for better characterizing ABI and its role in air quality degradation. A single column model (SCM) is used for sensitivity tests considering the balance between model performance and computational cost. This optimized grid setting is then applied in three-dimensional air quality modelling in eastern China. Compared with default configuration, the optimized one is demonstrated to perform much better in characterizing temperature stratification and extreme fine particle ($PM_{2.5}$) concentration as well as its diurnal variation during haze episodes. Specifically, the averaged decrease in PBL height and increment in surface $PM_{2.5}$ concentration are about 5% and 20% while applying optimized setting, thereby reducing the mean bias from 30 to 5 $\mu g/m^3$ in $PM_{2.5}$ concentration. The improvements could be attributed mainly to more accurate profiles of aerosol and its heating effect, and thus stabilized lower atmosphere. The optimization of vertical grid setting could be applied to areas with high concentration of absorbing aerosols such as eastern China and India, which could help better predict extreme near-surface pollution episodes.

1. Introduction

Eastern China has been suffering from heavy and frequent winter haze pollution that features concentrated ambient fine particles in the past two decades, arousing deep concern in scientific community for its adverse impacts on many aspects (Chan and Yao, 2008; Ding et al., 2016; Gao et al., 2016; Ji et al., 2014; Zhang et al., 2016). The extremely large loadings of fine particulate matter ($PM_{2.5}$) leads to the deterioration of regional visibility and exerts adverse effects on human health as well as ecosystem (Kim et al., 2015). Moreover, high-concentration aerosols in the atmosphere have been found to substantially modify the radiation energy budget of the earth-atmosphere system through both direct light extinction and indirectly serving as cloud condensation nuclei (CCN) (IPCC, 2013). This perturbation and reallocation in energy budget between the land surface and the atmosphere would inevitably lead to modifications in atmospheric dynamics at regional and even global scale (Ding et al., 2016; Meehl et al., 2008; Menon et al., 2002; Qiu et al., 2017; Yu, 2002).

A number of studies have revealed that planetary boundary layer (PBL) processes play an important role in haze aggravation by influencing the vertical diffusion and dispersion of aerosol particles (Ding et al., 2013, 2016; Hu et al., 2014b; Miao et al., 2017; Ye et al., 2016). Further, radiatively-active aerosols in turn could interact with solar radiation and trigger a positive feedback between PBL and fine particle pollution, which has been defined as Aerosol – Boundary layer Interaction (ABI) (Ding et al., 2016; Huang et al., 2018; Quan et al., 2013; Wang et al., 2015a, 2018). To be specific, atmospheric aerosols block the insolation and then cool the land surface, accompanied with light-absorbing components such as black carbon (BC) heating the upper boundary layer simultaneously (Ding et al., 2016; Wang et al., 2018). The opposite air temperature responses over land and ocean caused by BC could also weaken the East Asian winter monsoon circulation and

* Corresponding author. Joint International Research Laboratory of Atmospheric and Earth System Sciences, School of Atmospheric Sciences, Nanjing University, Nanjing, 210023, China.
E-mail address: xinhuang@nju.edu.cn (X. Huang).

https://doi.org/10.1016/j.atmosenv.2019.04.042
Received 2 January 2019; Received in revised form 17 April 2019; Accepted 20 April 2019
Available online 22 April 2019
1352-2310/

decrease the wind speed in the boundary layer and lower troposphere (Lou et al., 2019). Yang et al. (2017) proposed an interaction between dust loading and wind speed over eastern China, which was associated with variations of dust-induced atmospheric heating and conducive to air stagnation of the lower atmosphere. Theoretically, ABI is characterized by upper-air warming and near-surface cooling, which is also confirmed by multi-year observational evidences (Huang et al., 2018). Such opposite temperature responses in upper and lower PBL generate an increasingly stable inversion, weakening the turbulent exchange and vertical dispersion of near-surface air pollutants. Along with less sensible heat from surface, the convective motions and evolution of PBL tend to be greatly suppressed, leading to enhanced accumulation of locally-emitted pollutants within the lowest atmosphere (Ding et al., 2016; Wang et al., 2018).

Global and regional air quality models have been widely applied to analyze and predict haze pollution (Carmichael and Peters, 1986; Gong et al., 1997; Huang et al., 2013; Silibello et al., 2008; Wang et al., 2000; Ye et al., 2016). However, most of prevailing air quality forecast systems have not explicitly considered effects of aerosol on radiation, atmospheric thermal structure and cloud microphysics yet, which may modify the physical state of the atmosphere and hence impact the weather and the occurrence of pollution. Meanwhile, existing modelling studies already suggested that the exclusion of aerosol's radiative effect cannot well capture stable atmospheric stratification in most cases, which leads to a substantial underestimation of near surface particle concentration (Ding et al., 2016; Feingold, 2005; Petaja et al., 2016; Wang et al., 2015a). For instance, only when aerosol's feedback to PBL meteorology are considered can the model well reproduce the local convection, regional circulation and precipitation pattern during biomass burning season in eastern China (Ding et al., 2013; Huang et al., 2016). As aforementioned, since both numerical simulations and observational analysis are indicative of the importance of ABI and its impacts on pollution aggravation, it is necessary to accurately depict it in current air quality modelling in an efficient way for more in-depth understanding of haze pollution and better air quality forecasting.

The model vertical resolution has been demonstrated to exert great impact on simulating PBL processes. Tompkins and Emanuel (2000) reported significant errors in both water vapor and temperature profiles when using coarse resolution and highlighted the importance of resolving physical processes in PBL. Decreased biases in surface winds and atmospheric stability as well as boundary layer height were shown with the refinement of vertical resolution (Byrkjedal et al., 2007). Modelling studies have also pointed out the radiation fluxes at the surface, especially longwave radiation could be changed by up to 10% if there is poor resolution in boundary layer, hence influencing the continental and marine cloud formation and coverage in general circulation models (GCM) (Bushell and Martin, 1999; C. J. Somerville and Iacobellis, 2000; Räisänen, 2016). In addition, the onset and evolution of fog obtained with higher resolution are in better agreement with available observations due to better representation of key thermodynamical processes (Tardif, 2007). Particularly, the simulations of mesoscale convective systems suggested that increasing vertical resolution in different levels may result in different intensity of hurricane, indicating that a tailored vertical grid setting may stand out when simulating a specific process (K. Kimball and Carroll Dougherty, 2006; Zhang and Wang, 2003).

The upper PBL and near surface layer are expected to be two critical levels when conducting numerical simulations to resolve the ABI. As the interface of the turbulent mixing layer and the free atmosphere, the upper PBL particularly the capping inversion is a crucial thermal stable layer at the top of PBL (Hong et al., 2006). Conventionally, pollutants are mostly confined under the capping inversion thus aerosols within PBL is much more condensed than those found in the free atmosphere (Li et al., 2015). Large gradient of temperature as well as aerosol concentration is generally evident near the upper PBL. Also, existing studies found that BC in the upper PBL is more effective in heating the surrounding air and triggering ABI than that in other levels (Ding et al., 2016), and even more essential when BC mixed with other scattering aerosols, which is quite ubiquitous in winter haze events (Wang et al., 2018). On the other hand, the land–surface exchange processes for heat, moisture and momentum are vigorous in near surface layer, which is the bottom 5–10% of PBL. Featuring large gradients of variables (temperature, moisture, etc.) and substances (gases and aerosols), near surface layer is also associated with the development of PBL via transmission of thermal and momentum fluxes (Businger et al., 1971) and closely related to surface air quality and human health. Therefore, both of these two layers deserve additional concerns when performing air quality simulations. However, vertical grid setting in current air quality models is relatively coarse with typically 12–56 vertical levels for the total atmosphere column, the majority of which have only 4–8 layers below the 850 hPa level of the atmosphere (IPCC, 2013). The grid spacing decreases progressively with altitude, leaving no emphasis on the key levels of ABI, which is highly possible to introduce great bias when simulating such subtle structure of temperature stratification and pollutant profiles and thereby vertical diffusion within PBL.

To better characterize ABI in current air quality models, this paper suggests a key level-targeted vertical grid setting to more accurately simulate ABI and its role in haze aggravation. Compared with homogeneously putting more layers in the lower atmosphere, it is more efficient and computationally-inexpensive to only add more layers at some critical levels. The optimized vertical grid setting was first tested in a one-dimensional (1-D) WRF-Chem model and then applied to three-dimensional (3-D) model for regional scale simulations. The modelling results from conventional and optimized vertical grid settings were evaluated using multi-site observations to demonstrate the improvements in model performance. The paper is organized as follows. The observational data and methods are described in Section 2. Section 3 analyses results from 1-D ideal modelling as well as 3-D real case modelling with conventional and optimized vertical grid settings. The ability of two resolutions to capture the peak of $PM_{2.5}$ concentration and its diurnal variations are also discussed. Conclusions are summarized in Section 4.

2. Methodology

2.1. Observational data

The observed hourly mass concentration of $PM_{2.5}$ at individual ground-based monitoring sites for more than 74 major cities are obtained through the online access (http://datacenter.mep.gov.cn, last access: November 2018). This database is publicly released by the Ministry of Ecology and Environment (MEE) of People's Republic of China, which is quite essential for providing a more detailed picture of the extent of current air pollution situation in China and has been used in many previous studies (Hu et al., 2014a; Wang et al., 2014b). To obtain the surface meteorological conditions, station observations were acquired from the Global Surface Hourly database distributed by the US National Climate Data Center (NCDC) for December 2013. Four main cities including Beijing (40.08 °N, 116.58 °E), Zhengzhou (34.52 °N, 113.84 °E), Nanjing (31.74 °N, 118.82 °E), and Xi'an (34.45 °N, 108.7 °E) were extracted since hourly reports were only available at few sites. Air temperature at 2 m during polluted episodes was compared with model outputs by statistical analysis to evaluate the model's performance to reproduce the meteorological fields.

The radiosonde data at Beijing (39.94 °N, 116.36 °E, WMO station number 54511), Xuzhou (34.28 °N, 117.15 °E, WMO station number 58027) and Nanjing (32.00 °N, 118.80 °E, WMO station number 58238) observatories were collected from the University of Wyoming (http://weather.uw-yo.edu/upperair/sounding.html, last access: November 2018). The radiosondes were launched twice a day (08:00 and 20:00 LT) and measured profiles of atmospheric variables such as air temperature, water mixing ratio, wind speed, etc. The measurements are

Table 1
WRF-Chem regional and SCM modelling configuration options and settings.

	Domain setting	
	3D regional modelling	SCM
Horizontal grid	161 × 181	3 × 3
Grid spacing	20 km	4 km
Vertical layers	28/40	28/40/60
	Configurations	
Longwave radiation	RRTMG	
Shortwave radiation	RRTMG	
Land surface	Noah	
Boundary layer	YSU	
Microphysics	Lin et al.	
Cumulus parameterization	Grell-Deveny	
Photolysis	Fast-J	
Gas-phase chemistry	CBMZ	
Aerosol scheme	MOSAIC	

made both on the mandatory pressure levels (e.g., surface, 1000, 900, 850 hPa) and additional key levels.

2.2. WRF-Chem and model configurations

2.2.1. Real case regional modelling

The version 3.7 of Weather Research and Forecast Model with Chemistry (WRF-Chem) is employed in this study to conduct numerical experiments over eastern China. WRF-Chem is an online-coupled atmospheric model which simulates meteorology-chemistry-aerosol-radiation-cloud interactions via direct, semi-direct and indirect effects (Grell et al., 2005). Anthropogenic and biogenic emissions, photolysis, dry deposition and wet scavenging are all treated simultaneously with online meteorology. All transport processes related to atmospheric gases and aerosols including convective and turbulent transport as well as advection are all calculated by meteorological model with the same horizontal and vertical coordinates. The main configurations for WRF-Chem physical and chemical processes are listed in Table 1. A new version of the rapid radiative transfer model (RRTMG) for both long- and shortwave radiation (J. Iacono et al., 2008) was applied to perform radiation transfer within the atmosphere considering the feedback from aerosols to radiation schemes. The Yonsei University PBL scheme (YSU) (Hong et al., 2006) was implemented with Noah land surface scheme (Ek, 2003) to describe the diurnal evolution of PBL under the influence of aerosols as well as resolve land-atmosphere interactions. As for cloud and precipitation processes, Grell cumulus ensemble parameterization (Grell and Devenyi, 2002) along with Lin microphysics (Lin, 1983) scheme accounting for six forms of hydrometeor were employed in the simulation. The gas phase chemistry model used is based on the Carbon Bond Mechanism version Z (CBMZ) (Zaveri and Peters, 1999), which includes 67 species and 164 reactions in a lumped structure approach and organic compounds are classified according to their internal bond type. Photolytic reaction rates are derived using Fast-J photolysis scheme (Fast et al., 2006). The aerosol module is the Model for Simulating Aerosol Interactions and Chemistry (MOSAIC) (Zaveri et al., 2008) including 11 aerosol species, all of which are separated into 4 bins according to their dry diameter ranging from 0.039 to 10 μm. In each bin particles are assumed to be spherical and internally mixed. Aerosol optical properties, such as extinction coefficient, single scattering albedo (SSA) and asymmetry factor, were computed based on Mie theory. These options have been proved to perform well in simulating ABI process over eastern China (Ding et al., 2016; Huang et al., 2016).

The model domain is centered at 35.0 °N, 110.0 °E with a grid resolution of 20 km that covers eastern China and the surrounding regions. A total of 28 and 40 vertical levels extending from the surface to 50 hPa are utilized in the model, representing a conventional and an optimized vertical resolution respectively. Note that in optimized resolution more layers are placed in the upper PBL and near-surface inversion to better capture the boundary layer turbulent exchange and temperature modifications induced by aerosols. The initial and lateral boundary conditions of meteorological variables are obtained from National Center for Environment Prediction (NCEP) global final analysis data (FNL) with a 1° × 1° spatial resolution that update every 6 h. The lateral boundary conditions for chemistry fields are based on prescribed boundary profile. To investigate the improvements of optimized vertical resolution to simulate wintertime two-way feedback between aerosols and PBL and its impact on pollution aggravation, the simulations were conducted for the time period from 25th November to 26th December in 2013, when almost two thirds of China's territory experienced severe haze pollution (Ding et al., 2016; Jiang et al., 2015; Zhang, 2015). Each run covers 48 h and the last 24 h modelling results were used for further analysis. The chemical outputs from the previous run are used as the initial conditions for the following run. The first 6 days integration is considered as model spin-up period for atmospheric chemistry to minimize the influence of the initial conditions (Berge et al., 2001).

2.2.2. SCM ideal modelling and sensitivity experiments

The single column model (SCM) version of WRF-Chem is a one-dimensional, idealized model that includes all physical and chemical processes in the regional version except for advection (Wang et al., 2018). The SCM runs on a 3 × 3 grid with periodic lateral boundary conditions in both zonal and meridional directions. The grid is centered at Beijing (39.94 °N, 116.36 °E) with a spatial resolution of 4 km, which is more meticulous than the three-dimensional model but less computationally expensive. For its relative simplicity and computational attractiveness, SCM is often applied to conduct sensitivity tests. The physical and chemical parameterizations are configured the same as the regional model listed in Table 1. The initial conditions for SCM model are simply a meteorological sounding and a soil profile. In this study, three sets of parallel experiments (with/without ABI) using different vertical grid setting: conventional (28 layers), optimized (40 layers) and fine (60 layers) resolution are conducted, the last of which are considered as the appropriate solution. The detailed η values for three grid settings in WRF vertical coordinates are summarized in Table 2. We also tested the sensitivity of the results to other prevailing PBL parameterizations, such as turbulent kinetic energy (TKE) local closure scheme Mellor-Yamada-Janjic (MYJ) and Mellor-Yamada Nakanishi and Niino Level 2.5 (MYNN2.5), and the overall improvements of the

Table 2
Detailed η values for conventional, optimized and fine grid settings in WRF vertical coordinates.

Vertical resolution	Vertical grid η values
Conventional resolution (28 levels)	1.000, 0.976, 0.952, 0.926, 0.901, 0.880, 0.831, 0.783, 0.735, 0.687, 0.604, 0.528, 0.459, 0.398, 0.342, 0.292, 0.247, 0.207, 0.171, 0.139, 0.110, 0.086, 0.065, 0.048, 0.033, 0.020, 0.009, 0.000
Optimized resolution (40 levels)	1.000, 0.992, 0.985, 0.977, 0.969, 0.961, 0.952, 0.943, 0.934, 0.916, 0.896, 0.876, 0.865, 0.854, 0.843, 0.831, 0.819, 0.807, 0.795, 0.782, 0.769, 0.756, 0.728, 0.699, 0.668, 0.636, 0.602, 0.567, 0.529, 0.490, 0.448, 0.405, 0.359, 0.311, 0.261, 0.208, 0.152, 0.093, 0.032, 0.000
Fine resolution (60 levels)	1.000, 0.992, 0.985, 0.977, 0.969, 0.961, 0.952, 0.943, 0.934, 0.925, 0.916, 0.906, 0.896, 0.886, 0.876, 0.865, 0.854, 0.843, 0.831, 0.820, 0.808, 0.795, 0.782, 0.769, 0.756, 0.742, 0.728, 0.714, 0.699, 0.684, 0.669, 0.653, 0.636, 0.620, 0.603, 0.585, 0.567, 0.549, 0.530, 0.510, 0.490, 0.470, 0.449, 0.427, 0.405, 0.383, 0.360, 0.336, 0.312, 0.287, 0.261, 0.235, 0.208, 0.181, 0.152, 0.123, 0.094, 0.063, 0.032, 0.000

optimized resolution in these PBL schemes are consist with YSU scheme (Figs. S1 and S2).

2.2.3. Emission inventory

The Multi-resolution Emission Inventory for China (MEIC) developed by Tsinghua University (Li et al., 2014) was used in both regional real case modelling as well as SCM ideal experiments. Monthly anthropogenic emissions of SO_2, NO_x, CO, $PM_{2.5}$, PM_{coarse}, BC, OC and NMVOCs for five sectors (agriculture, industry, power plants, residential and transportation) are included with the finest resolution of $0.25^\circ \times 0.25^\circ$. A high-resolution ammonia emission inventory was applied over China (Huang et al., 2012). Non-methane organic compounds in MEIC were speciated into model-ready lumped species using profiles for Carbon Bond Mechanism (Hsu et al., 2006). As for one-dimensional experiments, regional-averaged emission of the North China Plain (NCP, i.e. Beijing, Tianjin and Hebei, the so-called Jing-Jin-Ji) was adopted to represent high intensity of anthropogenic activities in eastern China.

3. Results and discussions

3.1. Identification of key levels for ABI

By convention, there are approximately 4–8 vertical layers within PBL in prevailing air quality forecasting systems and their spacing usually decrease progressively along the altitude without any emphasis at key levels such as upper PBL or entrainment zone (IPCC, 2013; Jiang et al., 2015; Xian et al., 2019). Such vertical resolution of models are relatively coarse to resolve sophisticated physical processes in PBL, which are closely related to surface air quality and human health. As mentioned, atmospheric aerosols could interact with PBL meteorology and give rise to a positive feedback loop on pollutant concentration (Ding et al., 2013, 2016; Petaja et al., 2016). Characterized by substantial temperature and mass gradient, the upper PBL and near surface layer are expected to be two critical levels in aerosol-PBL interaction and should be paid more attention when conducting global and regional numerical simulation with chemistry (Ding et al., 2016; Huang et al., 2018; Wang et al., 2018). Thus, we conducted parallel simulations (with/without ABI) using three types of vertical grid settings in SCM so as to explore the proper resolution for depicting ABI. The disparities between experiments with and without ABI are considered as perturbations caused by aerosols, i.e. the effect of ABI. Accordingly, a key level-targeted vertical grid, namely optimized grid setting, which has more layers at two aforementioned levels, the upper PBL and near surface layer, was designed. At the same time, the simulations with conventional (28 layers, following default setting in WRF model) and fine (60 layers with vertical resolution of about 60 m/100 m within/above PBL) grid settings were also conducted for comparison. As illustrated in Fig. 1, the daily variation of air temperature and atmospheric stratification can be resolved reasonably well in all three sets of vertical grids. The air temperature peaks at noon and reaches the minimum around dawn. Notably, the air temperature at 2 m was about 1 °C at 4:00–8:00 LT in optimized and fine resolutions, but reached 4 °C in conventional resolution, suggesting that the inversion close to ground was weakened in the coarse grid. Such decreased stability of inversion may lead to inaccurate diffusion conditions and thereby undervalued pollutants concentration at nighttime (Han et al., 2009). The perturbation in air temperature caused by aerosols, namely upper level heating and surface cooling (Huang et al., 2018), can also be captured in all three vertical resolutions. However, the daily variation of the temperature responses in the optimized grid setting is closer to that in the fine resolution compared with the conventional one. The upper level heating caused by absorbing aerosols are 0.97, 1.11 and 1.12 °C in conventional, optimized and fine grid settings, respectively, indicating that the capability of the optimized grid setting to describe atmospheric heating induced by absorbing aerosols is as good as the fine resolution. Fig. 2 shows the air temperature profile and shortwave heating rate at 14:00 LT along with the vertical distribution of BC in experiments from three vertical resolutions. Due to deficient layers in the lower atmosphere, the conventional grid setting failed to reproduce the vertical profile of BC aerosols, with an underestimation of 40% (about 2.2 μg/m^3) at the upper PBL and overestimation of 10% (about 0.6 μg/m^3) in the whole middle PBL compared with the fine resolution, which could be regarded as the appropriate solution. The shortwave heating efficiency showed similar results that the optimized and fine resolution runs were quite close while the conventional one exhibited some discrepancies. The underrated shortwave heating rate at about 600 m is responsible for less significant temperature perturbation from conventional grid setting in Fig. 1. Additionally, the air temperature was greatly enhanced around 1000 m to about 1.5 °C in both optimized and fine resolution runs, while reached only 1.0 °C in conventional run with a weakened capping inversion.

Along with temperature perturbation, the vertical distribution of particulate matter (PM) can also be remarkably altered under the influence of ABI. The evolution of PBL has a significant impact on surface pollutant concentration since it directly determines the vertical dispersion and diffusion of gases and aerosols within the mixing layer (Miao et al., 2017; Quan et al., 2014). In turn, high-concentration aerosols block incoming solar radiation reaching the earth surface and enhance PBL stability, resulting in a lower PBL height and more aerosols condensed in a shallower layer (Ding et al., 2016; Huang et al., 2018; Petaja et al., 2016; Wang et al., 2018). The redistribution of PM caused by ABI in the vertical direction, i.e., increase of aerosol concentration within PBL and decrease above it, is clearly shown in Fig. 3. When excluding the radiative effect of aerosols, the daytime surface $PM_{2.5}$ concentration was about 170 μg/m^3, and the dry deposition velocity for aerosols were 1.98, 2.10 and 2.12 cm/s in three resolutions (Table 3). In contrast, the same resolutions but with ABI included demonstrated higher surface $PM_{2.5}$ concentrations, which were about 61.3, 69.6 and 70.1 μg/m^3 greater than experiments without ABI. The dry deposition velocity also declined by 0.5, 0.58 and 0.6 cm/s respectively, suggesting more stable stratification and less removal of particulate species from the atmosphere onto the earth surface. The decreased deposition rate and enhanced pollutant concentration are the typical influences of ABI, and obviously variations from optimized resolution agree better with the fine resolution, the latter of which could be viewed as the proper situation. In a word, the optimized grid setting has the ability to capture ABI and its impact on haze aggravation, and should thus be applied in the real case 3-D air quality modelling.

3.2. Implications in regional air quality modelling

Characterized by intense emission of air pollutants from the anthropogenic sources in megacity clusters, a half-open basin topography which is detrimental for pollutant diffusion, as well as unfavorable meteorological conditions, eastern China suffers from frequent and long-lasting regional air pollution problems in winter (Fig. 4a). As has been verified in 1-D simulations, the upper PBL and near surface layer are two important levels in modelling ABI and should be paid more attention when setting up vertical mesh grid to capture PBL processes considering ABI under heavily polluted conditions. In this study, the upper PBL is defined as a thick layer around the averaged PBL height diagnosed in YSU PBL scheme based on the vertical profile of bulk Richardson number during daytime (12:00–16:00 LT), while the near surface layer is defined as the layer around the inversion close to ground (where the air temperature peaks below 100 m) at nighttime (2:00–6:00 LT), both of which cover areas where variables vary rapidly along the altitude.

Due to the fact that radiosonde stations are relatively sparse (CMA sounding sites with an interval of several hundred kilometers in eastern China) and only detect profiles twice a day (08 and 20 LT), it is difficult to use sounding data to investigate the PBL structure over a large

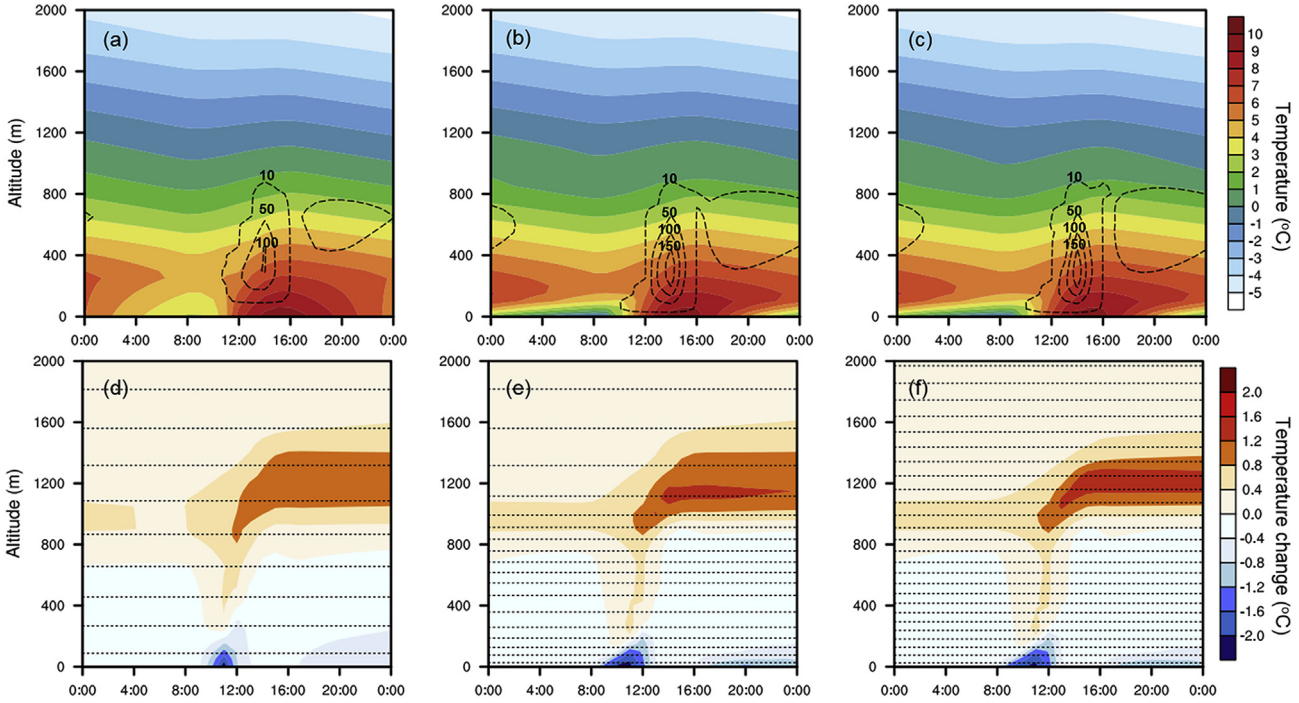

Fig. 1. Diurnal variation of air temperature vertical profile (upper panel) and its perturbation (lower panel) due to ABI in simulations from conventional (a, d), optimized (b, e) and fine (c, f) grid settings. The contour lines overlaid on the upper panel represent the exchange coefficient, while the dashed lines overlaid on the lower panel represent the vertical grid settings in three simulations.

domain owing to its low spatial and temporal resolution. Therefore, 4-year WRF simulations from 2013 to 2016 are conducted to acquire average winter daytime PBL height (Fig. 4b) and near surface layer height (not shown). The direct measurements such as temperature, humidity and wind from surface and radiosonde reports covering the entire domain were assimilated into the model every six hours through objective analysis to provide a superior estimate of the state of the atmosphere. The domain setting and model configurations are exactly the same as those described in Section 2.2. Fig. 5a–f presents the frequency distributions of the height, pressure and η value of upper PBL and near surface layer over the domain shown in Fig. 4, which is also the typical domain deployed when performing simulations concerning the eastern China. The daytime averaged PBL height mostly (60%) ranged from several hundred meters to 1 km, with a mean value of 574 m, which is comparable to PBL height derived from ERA Interim reanalysis data by Guo et al. (2016). In contrast, the nighttime averaged inversion layer height is more centralized with almost 50% presenting below 50 m. Optimized mesh grids are created to cover over 60% of their altitude

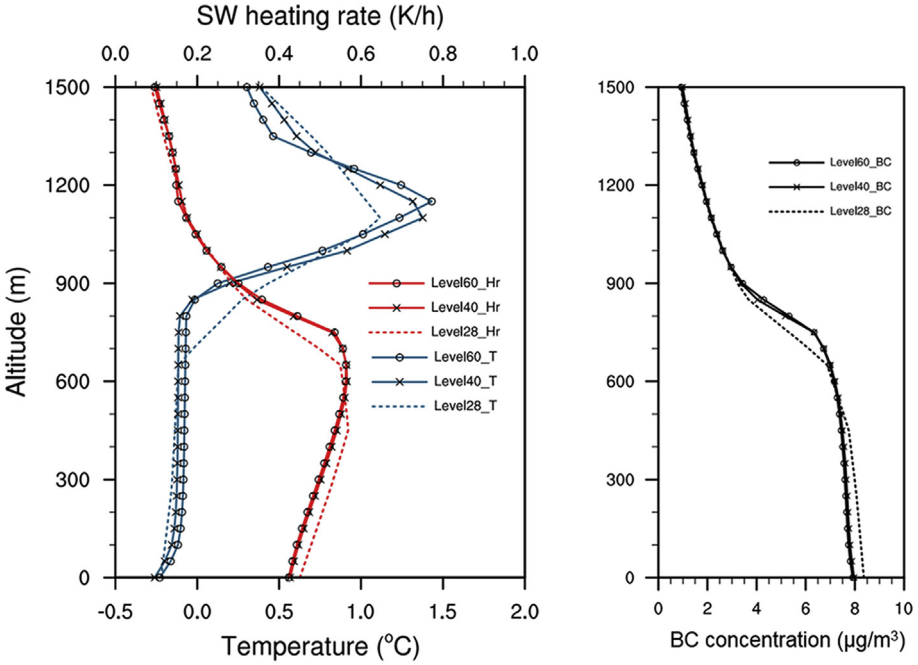

Fig. 2. Vertical profiles of air temperature, short wave radiation heating rate induced by BC and vertical distribution of BC aerosols at 14:00LT in three sets of vertical mesh grid. Circle-marked line, cross-marked line and dashed line stand for fine (Level60), optimized (Level40) and conventional (Level28) resolution, respectively.

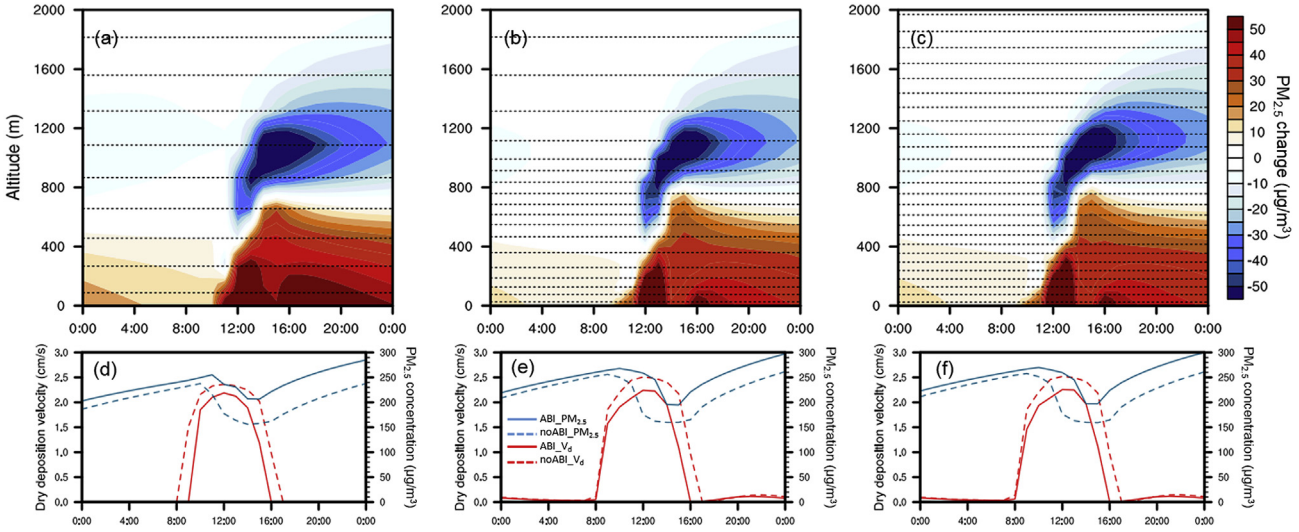

Fig. 3. Diurnal variation of $PM_{2.5}$ mass concentration perturbation due to ABI in simulations from conventional (a, d), optimized (b, e) and fine (c, f) grid settings. Their corresponding dry deposition velocity for aerosols (red lines) as well as surface $PM_{2.5}$ mass concentration (blue lines) are also shown in the lower panel, with dashed/solid lines for simulations without/with ABI. (For interpretation of the references to colour in this figure legend, the reader is referred to the web version of this article.)

Table 3
Surface $PM_{2.5}$ concentration and daytime dry deposition velocities from three vertical grid settings (Level28, Level40, Level60) in ABI and noABI scenarios.

	$PM_{2.5}$ (μg/m^3)		Deposition velocity (cm/s)	
	noABI	ABI	noABI	ABI
Level28	166.17	227.45	1.98	1.48
Level40	169.06	238.66	2.10	1.52
Level60	168.09	238.14	2.12	1.52

range and utilized to perform simulations of pollution episodes in the winter of 2013.

Several haze episodes occurred in eastern China during December of 2013, covering almost two thirds of China's territory (Ding et al., 2016). With daily mean observed $PM_{2.5}$ concentration over 200 μg/m^3, Jing-Jin-Ji region and the Yangtze River Delta (YRD) region were the most heavily polluted areas (Ding et al., 2016; Jiang et al., 2015; Liu et al., 2015; Wang et al., 2015b). The most intensive haze episodes on 2–8 (EP1) and 21–26 (EP2) December 2013 were selected to evaluate model's capability of describing extreme pollution events. The simulation results were first compared with the observational data from four major cities during the two haze episodes to assess the performance of conventional and optimized vertical grid settings. Generally, the simulated $PM_{2.5}$ concentrations were in good agreement with observations during the entire month, yet some discrepancies showed up when focusing on the pollution episodes (Fig. 6 and Fig. S4). During the first episode (EP1), the observed $PM_{2.5}$ concentration increased to about 350 μg/m^3 in Beijing in the afternoon of 7th December, which is about threefold larger than the daily averaged concentration stipulated by the

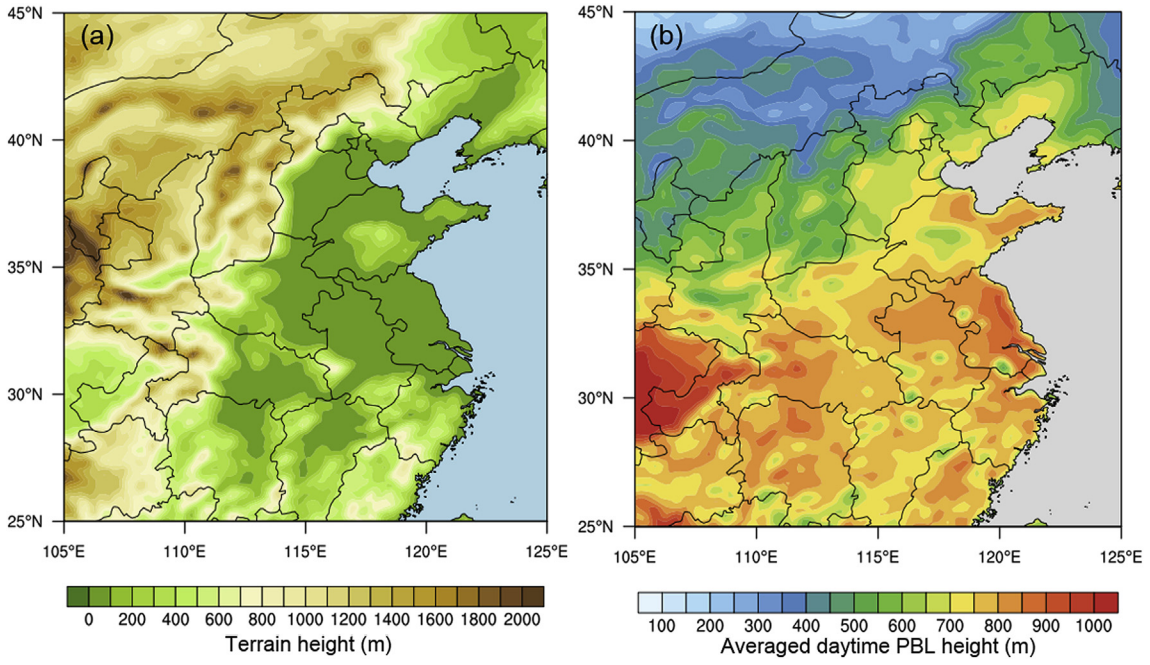

Fig. 4. Topography (a) and averaged daytime PBL height (b) of Eastern China from WRF-Chem simulations during the winter of 2013-2016.

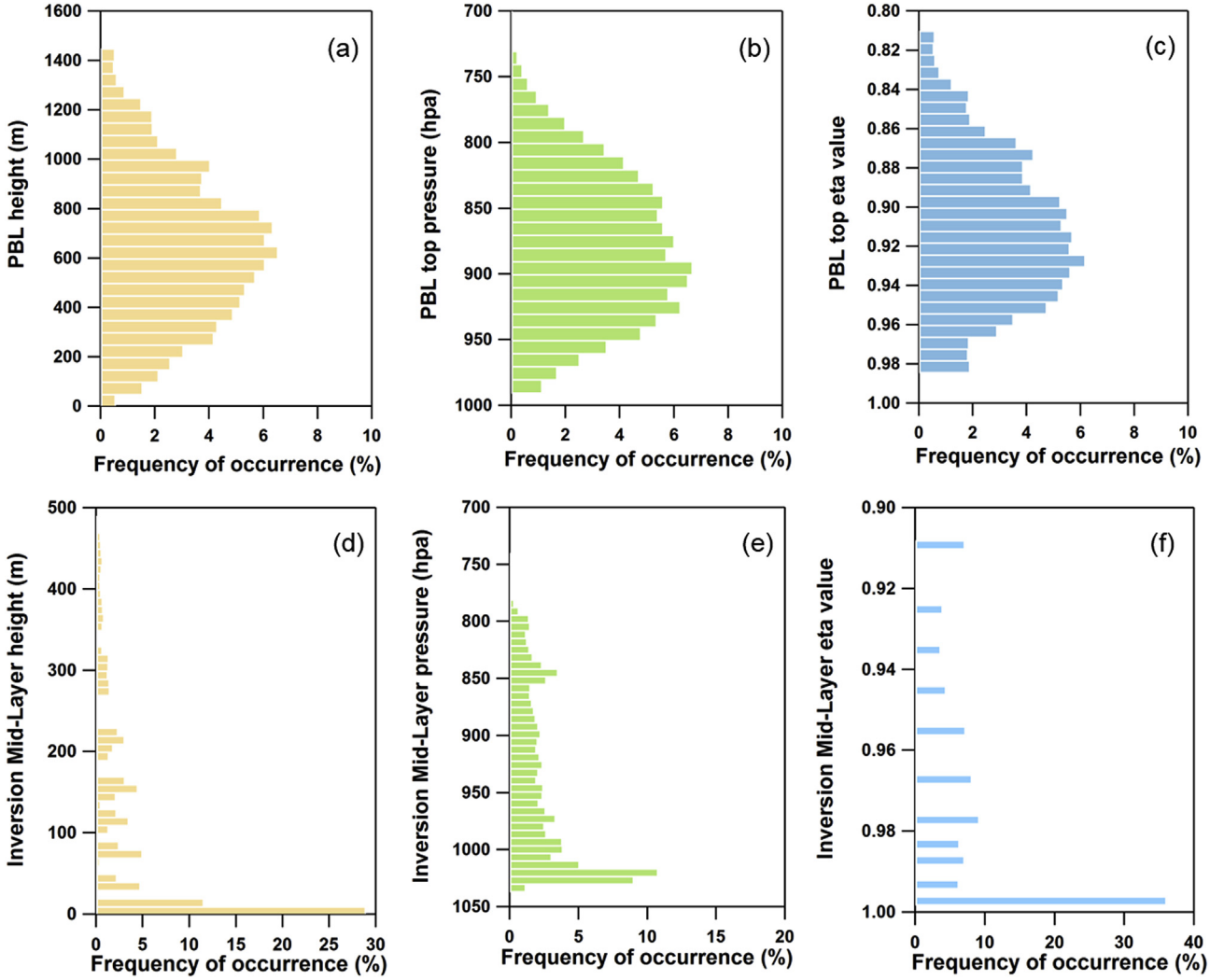

Fig. 5. Frequency distribution of daytime PBL height (a) and night-time inversion layer height (d) from WRF-Chem simulations during the winter of 2013-2016, along with their corresponding pressure (b, e) and η value (c, f) over the domain shown in Fig. 4.

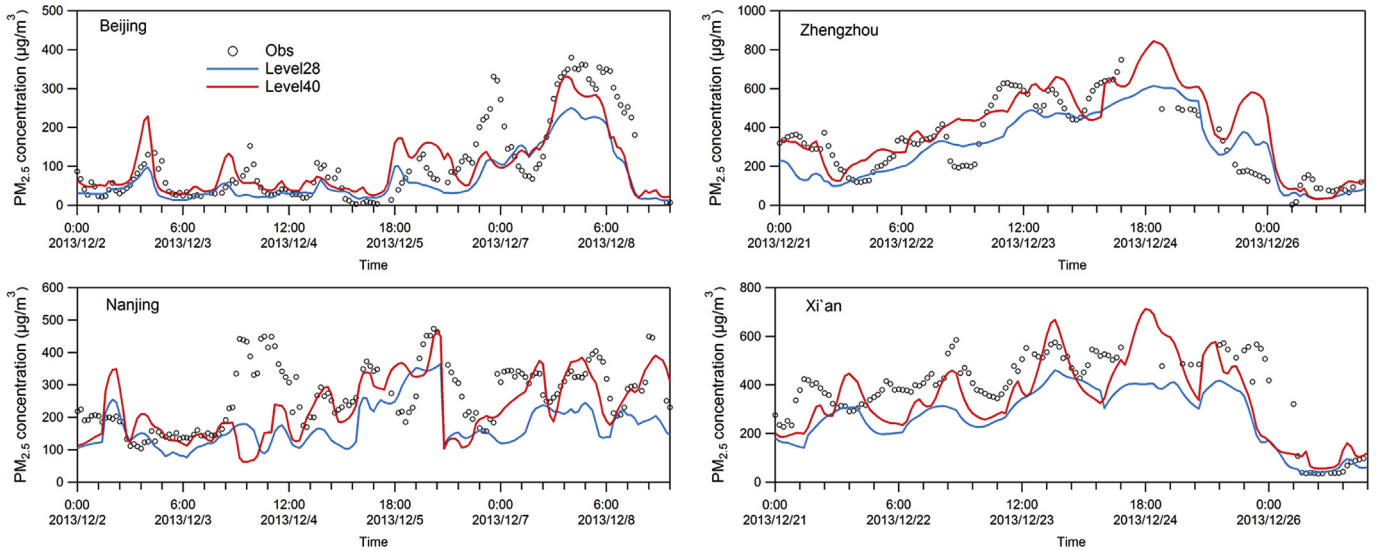

Fig. 6. Simulated hourly $PM_{2.5}$ mass concentration from two vertical grid settings compared with observations during two haze episodes (EP1 and EP2) in four typical cities: Beijing, Nanjing, Zhengzhou and Xi`an.

Grade II Air Quality National Standard (75 μg/m^3). The pollution was even more serious in Nanjing, capital of Jiangsu located in the west of YRD, suffering hourly observed maximum fine particle concentration reaching 400 μg/m^3 in three days of the episode. The averaged $PM_{2.5}$ observations through the episode were 115 and 265 μg/m^3 in Beijing and Nanjing, compared with 70, 174 μg/m^3 from conventional resolution and 100, 231 μg/m^3 from optimized resolution. Moreover, disparities of two resolutions were more obvious with greater observed aerosol loading, suggesting that the optimized grid setting is better at capturing PM concentration peaks and daily variations of pollutants, the latter of which would be further discussed in the following section. Owing to intensive local emissions combined with stagnant synoptic weather, the second episode (EP2) was characterized with continuous increase in the $PM_{2.5}$ concentrations over approximately four days in Zhengzhou and Xi'an. The accumulation and enhancement of aerosols were fairly reproduced by the optimized grid setting, while the conventional grid setting illustrated a negative bias of about 25%.

The spatial distribution of $PM_{2.5}$ concentration over the entire domain was also investigated. Owing to its short lifetime in the atmosphere, aerosol exhibited substantial spatial and temporal variations with peak concentration near emission sources. High concentration of $PM_{2.5}$ mainly occurred in eastern China, especially NCP and YRD, with the daily averaged maximum concentration exceeding over 250 μg/m^3. The feedback between aerosols and meteorological fields in the PBL could not only modulate the local scale processes like turbulent mixing but also exert an impact on the downwind pollutant transport across cities and even precipitation, which further influences the distribution of aerosol particles (Huang et al., 2016; Jiang et al., 2015). As shown in Fig. 7, large underestimation could be found over heavily polluted city clusters when excluding the effect of ABI (left panel). By comparison, simulations considering ABI (right panel) notably narrowed the gap with observations. To be specific, the normalized mean bias of $PM_{2.5}$ simulation during the haze pollution were −39.4% and −32.14% without the influence of aerosol in conventional and optimized resolution respectively, rising to −19.1% and 4.5% when considering the aerosol's radiative effect (Table S1), indicating the optimized grid setting is better at resolving pollution enhancement of ABI. Moreover, the conventional resolution failed to capture some peak values from the stations located in the northern part of NCP as well as the stations around Mount. Tai (Fig. S5). These subtle characteristics were all resolved by optimized grid setting with ABI effect included, which is also the best prediction of the actual PM spatial pattern. Overall, the averaged PBL height was declined by 5% in optimized grid setting compared with conventional resolution and near-surface fine particle concentration was enhanced by about 20% during the entire modelling period.

Meteorological variables, such as air temperature and relative humidity, are also of great importance in determining PBL thermodynamic properties, aerosol optical properties and some heterogeneous reactions. Statistical analyses of simulated air temperature at 2 m at four cities during pollution episodes (EP1 + EP2) are listed in Table 4. A great number of suspended aerosols could significantly block solar radiation in the atmosphere, leading to a decline of incoming solar energy and near surface air temperature (Ding et al., 2013; Huang et al., 2018; Yu, 2002). With a general under-prediction of aerosol concentration hence an undervalued extinction, it is not surprised to find a systematic positive bias of predicted air temperature at all cities when compared with in-situ measurements (Huang et al., 2018). In other words, the model tended to overestimate the radiation reaching surface, which resulted in the overestimation of near-surface air temperature. This discrepancy can be greatly reduced by applying optimized grid setting by more than 40%. The mean error and root mean square error of four cities were also decreased when utilizing the optimized resolution, implying less bias and higher accuracy of air temperature prediction.

Atmospheric stratification determines the stability of air masses as well as vertical turbulent mixing conditions of near surface pollutants. Both observations and simulations have found that aerosols could significantly alter the vertical temperature profile and the stability of the lower atmosphere (Ding et al., 2013, 2016; Huang et al., 2018; Wilcox et al., 2016). That is to say, the upper level heating by light-absorbing aerosols especially BC in the PBL and surface cooling by all extinctive aerosols result in more stabilized stratification. This modification of atmospheric stability caused by ABI should also be well described in the model because of its crucial contribution to air quality deterioration. Atmospheric sounding serves as a good way to detect the stratification and is analyzed to test the performance of models in reproducing the vertical temperature profile. Detected at 00UTC (8:00LT), the temperature profile is distinctively different from that at 12UTC (20:00LT), with a noticeable inversion layer located under 100 m (Fig. 8). Such an inversion layer is associated with the nighttime radiative cooling of the ground surface, revealed by the sounding in the morning when solar insolation is not sufficient to compensate the energy loss. On the contrary, the temperature decreased with height in most cases at 12UTC, indicating that the surface functions as a heating source for the air masses in the lower troposphere. With more layers near the ground, the optimized grid setting is better at resolving the inversion layer while the conventional configuration failed to characterize the inversion curvature due to less information of variables in the vertical direction (Byrkjedal et al., 2007). In addition, the upper level heating caused by absorption aerosols is clearly demonstrated in the optimized grid setting, which would otherwise be partly neglected when using conventional resolution (Fig. S6). The reasons for the heating promotion can be attributed to two factors. Firstly, the vertical distribution of aerosols is more accurate with more layers at upper PBL to resolve horizontal transport of aerosol plumes and emissions from elevated point sources. And the aerosol profile is a key parameter that influences the strength of ABI because of its sensitivity to the altitude of aerosol layer (Wang et al., 2018). With higher resolution, the turbulent exchange of aerosols and heating efficiency at key levels of the atmosphere could be more exact. Secondly, poor vertical resolution could result in excessive vertical diffusion of heat as a result of the implicit diffusion operating in the vertical advection schemes (Tompkins and Emanuel, 2000). Noted that the atmospheric heating usually appears at 12UTC since the aerosol interacts with radiation only during daytime.

3.3. Capability in simulating extreme pollution episode and its diurnal cycle

The underestimation of pollutants especially aerosol concentrations is one of the common problems when performing haze predictions or simulations (Wang et al., 2013, 2014a). To gain more insights of the models' ability to capture extreme haze episodes as well as the diurnal variation of aerosols, hourly $PM_{2.5}$ mass concentrations on polluted days of two episodes (EP1 + EP2) are analyzed. Fig. 9 shows the relationship between observed hourly $PM_{2.5}$ concentration and their corresponding residual, which is defined as the differences between simulations and observations for both conventional and optimized resolution. Linear fitting curve for two resolutions are given as well. While remaining small below 100 μg/m^3, the residual grows larger with higher loadings of fine particles. The averaged deviation of red dots (optimized) is relatively limited and fluctuated mostly around the zero line. However, blue dots (conventional) are more dispersed and located around an oblique line with a slope of −0.39, indicating a more serious underestimation of near surface pollutants under heavily polluted situations. In other words, such optimized grid setting improves PM simulation more efficiently during severely polluted episodes. The improvements can be attributed to better resolved aerosol vertical distribution and its interaction with radiation, as well as PBL processes affected by ABI such as vertical turbulent mixing.

The performance of air quality models on characterizing pollutants diurnal variation is of great importance for assessing human exposure to air pollution as well as regional climate since daytime pollution is more closely related to human health and shortwave radiative effect of

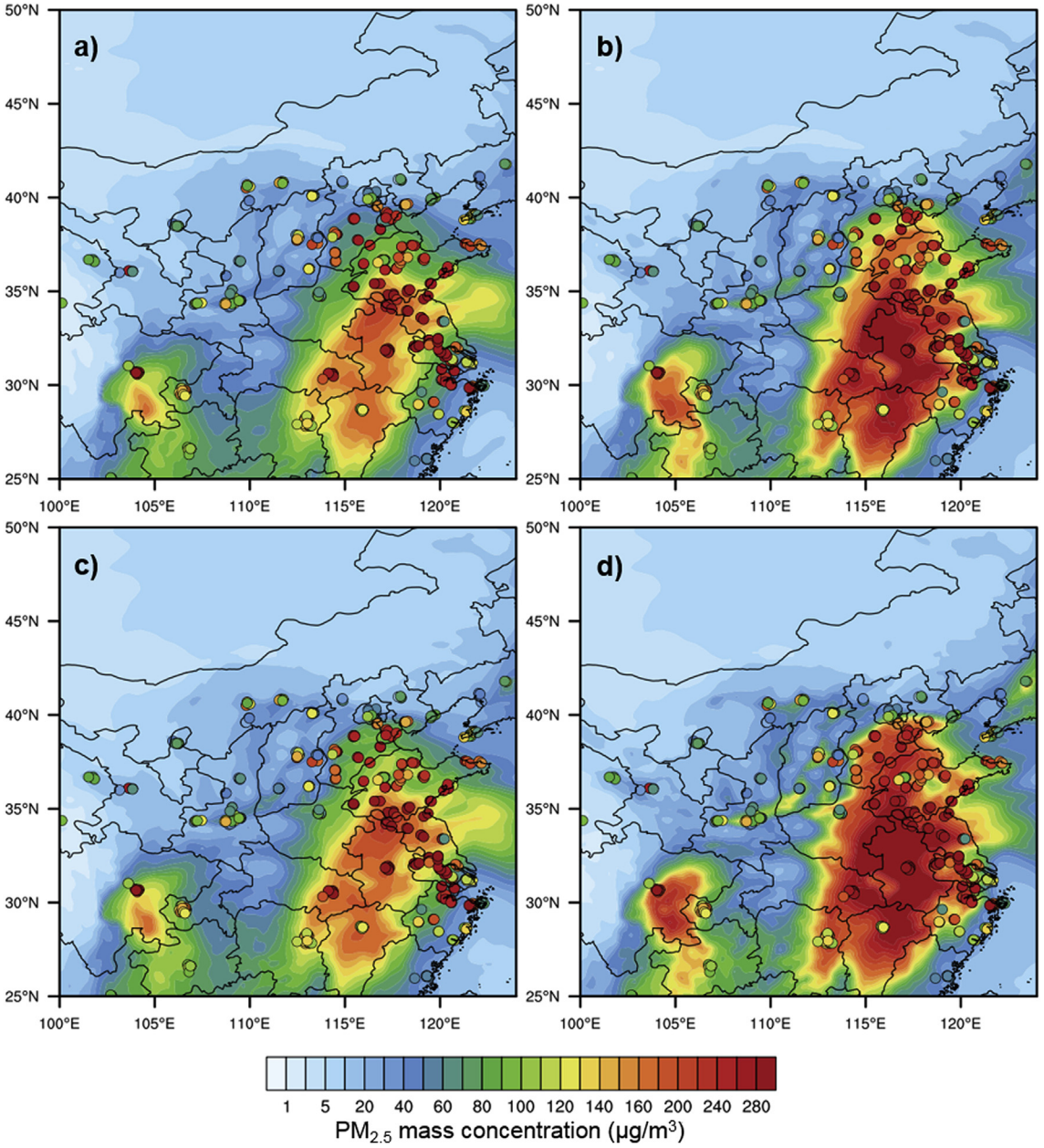

Fig. 7. Observed (circles) and simulated daily mean $PM_{2.5}$ mass concentration with conventional (a without ABI, b with ABI) and optimized (c without ABI, d with ABI) vertical grid settings over the eastern China on 4th December, 2013.

Table 4
Statistical analyses of the simulated 2 m temperature and the corresponding observations at four cities (Beijing, Zhengzhou, Nanjing, Xi'an) during polluted episodes from conventional (L28) and optimized (L40) resolution.

	MB[a]		ME[a]		RMSE[a]	
	L28	L40	L28	L40	L28	L40
BJ	−0.46	−0.15	2.44	2.23	2.90	2.61
ZZ	−0.52	−0.27	2.07	1.88	2.6	2.37
NJ	−0.92	−0.61	1.48	1.53	2.23	1.97
XA	−0.91	−0.42	1.71	1.46	2.31	1.97

[a] MB, ME and RMSE refer to mean bias, mean error and root-mean-square error respectively.

aerosols. The diurnal variation of near surface pollutants is regulated by a combination of the development of PBL associated with changing solar insolation and the variation of emission intensity associated with anthropogenic activities such as residential cooking and transportations (Quan et al., 2013; Tie et al., 2007). Conventionally, the PBL height peaks at noon and reaches a relatively stable minimum at night. Higher PBL height favors the vertical diffusion of near-surface pollutants. Taking an urban monitoring station of Beijing for instance, the observed $PM_{2.5}$ diurnal variations during two polluted episodes clearly demonstrated a minimum after 12:00 LT and a maximum at night (Fig. 10b). The morning and evening peaks are related to residential and rush-hour transportation emissions in downtown area. Generally, the model with optimized grid setting shows better agreement with observations, and the daytime averaged concentration had similar magnitude as the observed fine particle values. The more accurately shaped $PM_{2.5}$ diurnal variations were related to better resolved near surface stable layer in the morning and evening (8:00–9:00 and 19:00–21:00 LT in Fig. 10),

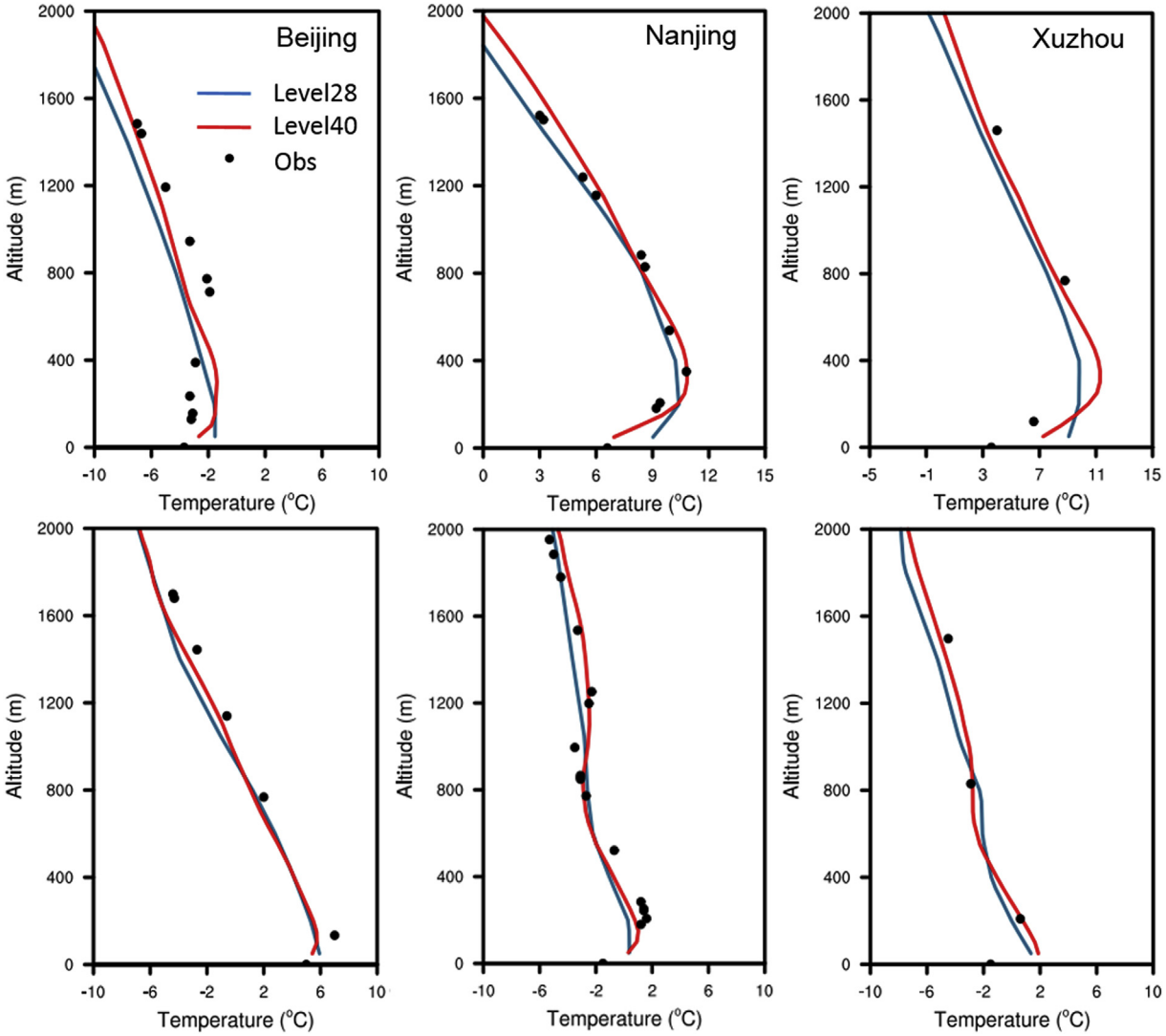

Fig. 8. Air temperature profiles observed by radiosonde (dots) at 00 and 12 UTC (08 and 20 LT) during polluted episodes and simulations from conventional (blue) and optimized (red) grid settings. (For interpretation of the references to colour in this figure legend, the reader is referred to the web version of this article.)

and thereby limited dispersal volume for polluted gases and aerosols, which could be easily affected by intensive local emissions in rush hours. On the other hand, the observed $PM_{2.5}$ in Huairou, a northeastern suburban station, showed totally different diurnal pattern. Instead of reaching a minimum at noon, it peaks in the afternoon (about 13:00LT) and evening (about 20:00LT) with two distinct elevated processes before. As the anthropogenic emission is much less intensive, suburban areas are less polluted and high concentration of aerosols are more tied to regional transport (Gao et al., 2017), horizontally as well as vertically. With the constantly developing PBL in the morning, plumes transported by southerly wind from urban areas above capping inversion were entrained into the PBL and spread down through turbulent mixing, thereby increasing the particle concentration near the ground surface. As the surface heating the atmosphere, the development of PBL is finally enough to dilute the particles within it, leading to a reduction in near surface pollutants. Shortly after sunset, the PBL quickly falls down and condenses the column aerosols into a shallow layer, giving rise to the second peak. With more layers set around the top of PBL, the $PM_{2.5}$ simulations at suburban stations in optimized configuration also agreed well with observations owing to the capture of regional transport plume and entrainment at the interface of mixing layer and free atmosphere (Xu et al., 2018). By contrast, the conventional grid setting showed no significant diurnal pattern and lower nighttime PM concentration in both urban and suburban stations, which is likely due to the missing of ground inversion layer as well as deficient entrainment at the top of PBL and thereby inappropriate aerosol vertical diffusion conditions. However, the PM concentration from both grid settings showed larger errors at nighttime than daytime, which may be related to the failure of PBL parameterization depicting nocturnal stable PBL processes and need further investigation.

4. Summary and conclusions

Atmospheric aerosols could perturb the radiation transfer and hence influence PBL meteorology, thereby significantly enhancing the near-surface haze pollution. However, most of current air quality simulations have not explicitly included or cannot well represent such kind of interaction when performing air quality forecast or pollution processes analyses, which may often lead to substantial underestimation of atmospheric stability and near-surface pollutants' concentration. Since the aforementioned processes are closely related to the vertical characterization and resolving of PBL, in this study, 1-D meteorological PBL – chemistry online coupled model was applied to verify the key levels of PBL processes under the impact of ABI. The upper PBL and near surface layer were identified as two critical levels which cover the area with large gradient of variables and crucial physical processes and need extra

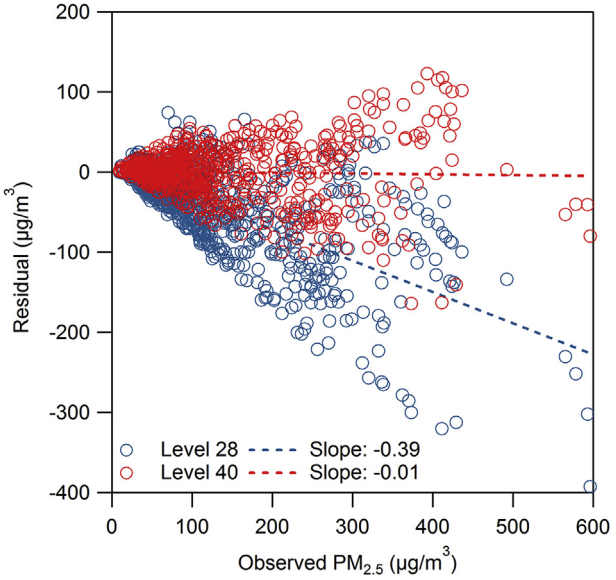

Fig. 9. Scatter plot between observed hourly $PM_{2.5}$ concentrations and their residual compared with modelling results at Beijing during two polluted episodes. The blue and red dashed line are linear fitting curves for conventional and optimized simulations, respectively. (For interpretation of the references to colour in this figure legend, the reader is referred to the web version of this article.)

attention when conducting numerical simulations. The experiments showed that with more layers at these two key levels, referred to as optimized grid setting, the model performance on vertical profile of air temperature and aerosols in the model was greatly improved, comparable to results from the finest resolution. The upper level heating caused by absorbing aerosols was enhanced up to 15%. As a consequence, air temperature in the upper PBL increased from 1 to 1.5 °C, equivalent to 30% intensification of atmospheric stability. Furthermore, almost all of surface $PM_{2.5}$ concentration change and dry deposition velocity change caused by ABI in the accurate situation could be reproduced in the optimized configuration, yet only 80% were captured in conventional resolution. Such improvements were of critical importance for haze predictions and simulations.

The optimized vertical grid setting derived from statistical analyses over the entire domain was then applied in the 3-D air quality modelling in eastern China. Compared with default resolution, the optimized run is demonstrated to perform much better at capturing temperature stratification and extreme fine particle concentration values as well as its diurnal variation during pollution episodes. Specifically, the averaged decrease in PBL height and increment in surface $PM_{2.5}$ concentration are about 5% and 20% while applying the optimized setting, thereby reducing the bias from 30 to 5 $\mu g/m^3$ in $PM_{2.5}$ concentration reproduction. Moreover, the overestimation of near surface temperature can be greatly reduced by more than 40%. The improvement can be attributed to better-resolved atmospheric stratification and shortwave heating efficiency.

In this work, we mainly focused on eastern China where severe haze pollution occurred in the wintertime. The frequency distribution of daytime PBL height and surface inversion layer over this region was derived from persistent regional WRF-Chem modelling, which was then used to create optimized mesh grids covering over 60% of the altitude variation of PBL height and inversion layer. Due to factors such as large-scale atmospheric motion, fluctuating surface fluxes, underlying land-use and topography, the daytime evolution of PBL varies substantially both in time and space, making the definition of the upper PBL somewhat flexible. However, the idea of increasing vertical resolution at key levels of ABI and the method to derive the optimized vertical grids could be extended and applied to other areas under the influence of ABI with global reanalysis data such as ERA5 hourly data, which shows similar results with regional WRF-Chem modelling except for complex terrain and multifarious types of land-use (Fig. S3). Such an optimization of vertical grid setting in air quality model could help better predict extreme near-surface pollution in some specific areas with substantial loadings of absorbing aerosols (such as winter in eastern China, dry season in northern India, etc.), and adopt quick prevention measures in current air quality forecast and emergency response system.

Acknowledgements

This work was supported by the National Natural Science Foundation of China (91544231, 41725020, 91744311, 41422504). Real-time air quality data across China were collected through the

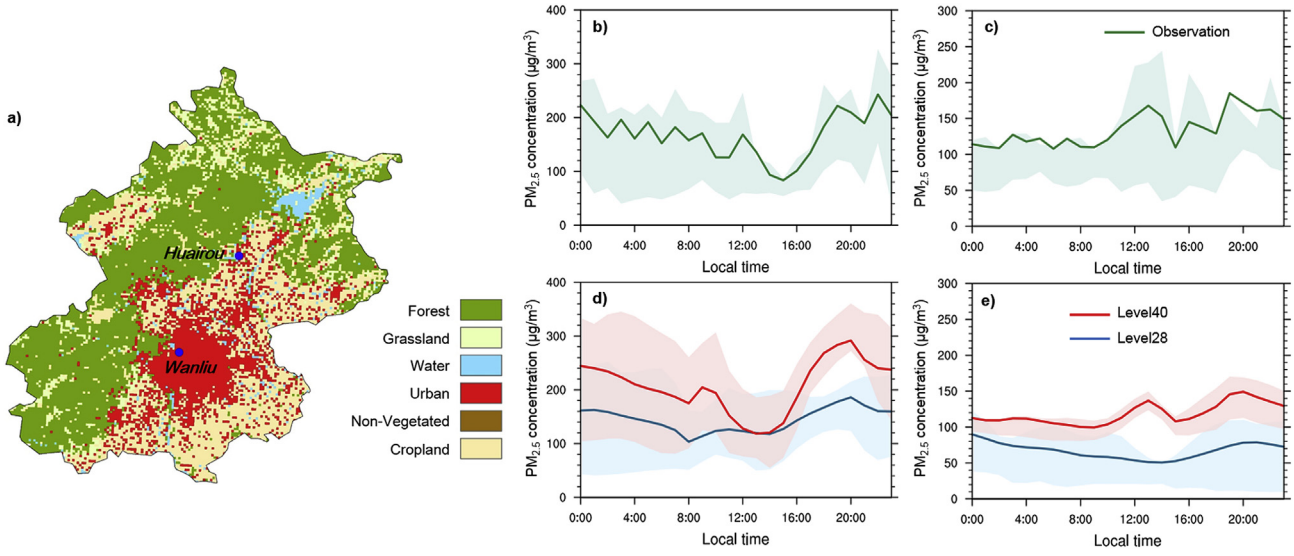

Fig. 10. Geographical locations of urban and suburban stations in Beijing overlaid by MODIS-retrieved land use map in 2010 (a). Observed (upper panel) and simulated (lower panel, blue for conventional, red for optimized) $PM_{2.5}$ diurnal variations during two polluted episodes at urban (b, d) and suburban (c, e) station. Solid lines and shaded area represent average, 25-75th percentile, respectively. (For interpretation of the references to colour in this figure legend, the reader is referred to the web version of this article.)

online access to ambient air monitoring data center (http://datacenter.me-p.gov.cn). The radiosonde observations are archived at http://weather.uwyo.edu/upper-air/sounding.html, and global hourly surface meteorological data are available at https://www.ncei.noaa.gov/da-ta/global-hourly/access/.

Appendix A. Supplementary data

Supplementary data to this article can be found online at https://doi.org/10.1016/j.atmosenv.2019.04.042.

References

Berge, E., Huang, H.-C., Chang, J., Liu, T.-H., 2001. A study of the importance of initial conditions for photochemical oxidant modeling. J. Geophys. Res.: Atmosphere 106, 1347–1363.

Bushell, A.C., Martin, G.M., 1999. The impact of vertical resolution upon GCM simulations of marine stratocumulus. Clim. Dyn. 15, 293–318.

Businger, J.A., Wyngaard, J.C., Izumi, Y., Bradley, E.F., 1971. Flux-profile relationships in the atmospheric surface layer. J. Atmos. Sci. 28, 181–189.

Byrkjedal, Ø., Esau, I., Kvamstø, N.G., 2007. Sensitivity of simulated wintertime Arctic atmosphere to vertical resolution in the ARPEGE/IFS model. Clim. Dyn. 30, 687–701.

Carmichael, G.R., Peters, L.K., 1986. A second generation model for regional-scale transport/chemistry/deposition. Atmos. Environ. 20, 173–188.

Chan, C.K., Yao, X., 2008. Air pollution in mega cities in China. Atmos. Environ. 42, 1–42.

Ding, A.J., Fu, C.B., Yang, X.Q., Sun, J.N., Petäjä, T., Kerminen, V.M., Wang, T., Xie, Y., Herrmann, E., Zheng, L.F., Nie, W., Liu, Q., Wei, X.L., Kulmala, M., 2013. Intense atmospheric pollution modifies weather: a case of mixed biomass burning with fossil fuel combustion pollution in eastern China. Atmos. Chem. Phys. 13, 10545–10554.

Ding, A.J., Huang, X., Nie, W., Sun, J.N., Kerminen, V.M., Petäjä, T., Su, H., Cheng, Y.F., Yang, X.Q., Wang, M.H., Chi, X.G., Wang, J.P., Virkkula, A., Guo, W.D., Yuan, J., Wang, S.Y., Zhang, R.J., Wu, Y.F., Song, Y., Zhu, T., Zilitinkevich, S., Kulmala, M., Fu, C.B., 2016. Enhanced haze pollution by black carbon in megacities in China. Geophys. Res. Lett. 43, 2873–2879.

Ek, M.B., 2003. Implementation of Noah land surface model advances in the National Centers for Environmental Prediction operational mesoscale Eta model. J. Geophys. Res. 108.

Fast, J.D., W.I.G Jr., , Easter, R.C., Zaveri, R.A., Barnard, J.C., Chapman, E.G., Grell, G.A., Peckham, S.E., 2006. Evolution of ozone, particulates, and aerosol direct radiative forcing in the vicinity of Houston using a fully coupled meteorology-chemistry-aerosol model. J. Geophys. Res. Atmos. 111, 5173–5182.

Feingold, G., 2005. On smoke suppression of clouds in Amazonia. Geophys. Res. Lett. 32.

Gao, M., Carmichael, G.R., Wang, Y., Saide, P.E., Yu, M., Xin, J., Liu, Z., Wang, Z., 2016. Modeling study of the 2010 regional haze event in the North China Plain. Atmos. Chem. Phys. 16, 1673–1691.

Gao, M., Liu, Z., Wang, Y., Lu, X., Ji, D., Wang, L., Li, M., Wang, Z., Zhang, Q., Carmichael, G.R., 2017. Distinguishing the roles of meteorology, emission control measures, regional transport, and co-benefits of reduced aerosol feedbacks in “APEC Blue”. Atmos. Environ. 167, 476–486.

Gong, S.L., Barrie, L.A., Blanchet, J.P., 1997. Modeling sea-salt aerosols in the atmosphere: 1. Model development. J. Geophys. Res.: Atmosphere 102, 3805–3818.

Grell, G., Devenyi, D., 2002. A Generalized Approach to Parameterizing Convection Combining Ensemble and Data Assimilation.

Grell, G.A., Peckham, S.E., Schmitz, R., McKeen, S.A., Frost, G., Skamarock, W.C., Eder, B., 2005. Fully coupled “online” chemistry within the WRF model. Atmos. Environ. 39, 6957–6975.

Guo, J., Miao, Y., Zhang, Y., Liu, H., Li, Z., Zhang, W., He, J., Lou, M., Yan, Y., Bian, L., Zhai, P., 2016. The climatology of planetary boundary layer height in China derived from radiosonde and reanalysis data. Atmos. Chem. Phys. 16, 13309–13319.

Han, S., Bian, H., Tie, X., Xie, Y., Sun, M., Liu, A., 2009. Impact of nocturnal planetary boundary layer on urban air pollutants: measurements from a 250-m tower over Tianjin, China. J. Hazard Mater. 162, 264–269.

Hong, S.-Y., Noh, Y., Dudhia, J., 2006. A New Vertical Diffusion Package with an Explicit Treatment of Entrainment Processes.

Hsu, Y., Strait, R., Roe, S., Holoman, D.S., 2006. 4.0. Speciation Database Development Documentation. Final Report. U.S. Environmental Protection Agency.

Hu, J., Wang, Y., Ying, Q., Zhang, H., 2014a. Spatial and temporal variability of PM2.5 and PM10 over the north China plain and the Yangtze River Delta, China. Atmos. Environ. 95, 598–609.

Hu, X.M., Ma, Z., Lin, W., Zhang, H., Hu, J., Wang, Y., Xu, X., Fuentes, J.D., Xue, M., 2014b. Impact of the Loess Plateau on the atmospheric boundary layer structure and air quality in the North China Plain: a case study. Sci. Total Environ. 499, 228–237.

Huang, X., Song, Y., Li, M., Li, J., Huo, Q., Cai, X., Zhu, T., Hu, M., Zhang, H., 2012. A high-resolution ammonia emission inventory in China. Glob. Biogeochem. Cycles 26.

Huang, K., Fu, J.S., Hsu, N.C., Gao, Y., Dong, X., Tsay, S.-C., Lam, Y.F., 2013. Impact assessment of biomass burning on air quality in Southeast and East Asia during BASE-ASIA. Atmos. Environ. 78, 291–302.

Huang, X., Ding, A., Liu, L., Liu, Q., Ding, K., Niu, X., Nie, W., Xu, Z., Chi, X., Wang, M., Sun, J., Guo, W., Fu, C., 2016. Effects of aerosol–radiation interaction on precipitation during biomass-burning season in East China. Atmos. Chem. Phys. 16, 10063–10082.

Huang, X., Wang, Z., Ding, A., 2018. Impact of aerosol-PBL interaction on haze pollution: multiyear observational evidences in north China. Geophys. Res. Lett. 45, 8596–8603.

Iacono, J., Delamere, M.,S., Mlawer, J.,J., Shephard, M., Clough, S., Collins, W., 2008. Radiative Forcing by Long-Lived Greenhouse Gases: Calculations with the AER Radiative Transfer Models.

IPCC, 2013. Climate Change 2013: the Physical Science Basis. Contribution of Working Group I to the Fifth Assessment Report of the Intergovernmental Panel on Climate Change. Cambridge University Press, Cambridge, United Kingdom and New York, NY, USA.

Ji, D., Li, L., Wang, Y., Zhang, J., Cheng, M., Sun, Y., Liu, Z., Wang, L., Tang, G., Hu, B., Chao, N., Wen, T., Miao, H., 2014. The heaviest particulate air-pollution episodes occurred in northern China in January, 2013: insights gained from observation. Atmos. Environ. 92, 546–556.

Jiang, C., Wang, H., Zhao, T., Li, T., Che, H., 2015. Modeling study of $PM_{2.5}$ pollutant transport across cities in China's Jing–Jin–Ji region during a severe haze episode in December 2013. Atmos. Chem. Phys. 15, 5803–5814.

Kim, K.-H., Kabir, E., Kabir, S., 2015. A review on the human health impact of airborne particulate matter. Environ. Int. 74, 136–143.

Kimball, S.K., Carroll Dougherty, F., 2006. The Sensitivity of Idealized Hurricane Structure and Development to the Distribution of Vertical Levels in MM5.

Li, M., Zhang, Q., Streets, D.G., He, K.B., Cheng, Y.F., Emmons, L.K., Huo, H., Kang, S.C., Lu, Z., Shao, M., Su, H., Yu, X., Zhang, Y., 2014. Mapping Asian anthropogenic emissions of non-methane volatile organic compounds to multiple chemical mechanisms. Atmos. Chem. Phys. 14, 5617–5638.

Li, J., Fu, Q., Huo, J., Wang, D., Yang, W., Bian, Q., Duan, Y., Zhang, Y., Pan, J., Lin, Y., Huang, K., Bai, Z., Wang, S.-H., Fu, J.S., Louie, P.K.K., 2015. Tethered balloon-based black carbon profiles within the lower troposphere of Shanghai in the 2013 East China smog. Atmos. Environ. 123, 327–338.

Lin, Y.L., 1983. Bulk parameterization of the snow field in a cloud model. J. Clim. Appl. Meteorol. 22, 1065–1092.

Liu, X., Hui, Y., Yin, Z.-Y., Wang, Z., Xie, X., Fang, J., 2015. Deteriorating haze situation and the severe haze episode during December 18–25 of 2013 in Xi’an, China, the worst event on record. Theor. Appl. Climatol. 125, 321–335.

Lou, S., Yang, Y., Wang, H., Smith, S.J., Qian, Y., Rasch, P.J., 2019. Black carbon amplifies haze over the north China plain by weakening the east asian winter monsoon. Geophys. Res. Lett. 46, 452–460.

Meehl, G.A., Arblaster, J.M., Collins, W.D., 2008. Effects of black carbon aerosols on the Indian monsoon. J. Clim. 21, 2869–2882.

Menon, S., Hansen, J., Nazarenko, L., Luo, Y., 2002. Climate effects of black carbon aerosols in China and India. Science 297, 2250–2253.

Miao, Y., Guo, J., Liu, S., Liu, H., Li, Z., Zhang, W., Zhai, P., 2017. Classification of summertime synoptic patterns in Beijing and their associations with boundary layer structure affecting aerosol pollution. Atmos. Chem. Phys. 17, 3097–3110.

Petaja, T., Jarvi, L., Kerminen, V.M., Ding, A.J., Sun, J.N., Nie, W., Kujansuu, J., Virkkula, A., Yang, X.Q., Fu, C.B., Zilitinkevich, S., Kulmala, M., 2016. Enhanced air pollution via aerosol-boundary layer feedback in China. Sci. Rep. 6, 18998.

Qiu, Y., Liao, H., Zhang, R., Hu, J., 2017. Simulated impacts of direct radiative effects of scattering and absorbing aerosols on surface layer aerosol concentrations in China during a heavily polluted event in February 2014. J. Geophys. Res.: Atmosphere 122, 5955–5975.

Quan, J., Gao, Y., Zhang, Q., Tie, X., Cao, J., Han, S., Meng, J., Chen, P., Zhao, D., 2013. Evolution of planetary boundary layer under different weather conditions, and its impact on aerosol concentrations. Particuology 11, 34–40.

Quan, J., Tie, X., Zhang, Q., Liu, Q., Li, X., Gao, Y., Zhao, D., 2014. Characteristics of heavy aerosol pollution during the 2012–2013 winter in Beijing, China. Atmos. Environ. 88, 83–89.

Räisänen, P., 2016. The effect of vertical resolution on clear-sky radiation calculations: tests with two schemes. Tellus Dyn. Meteorol. Oceanogr. 48, 403–423.

Silibello, C., Calori, G., Brusasca, G., Giudici, A., Angelino, E., Fossati, G., Peroni, E., Buganza, E., 2008. Modelling of PM10 concentrations over Milano urban area using two aerosol modules. Environ. Model. Softw 23, 333–343.

Somerville, R.C.J., Iacobellis, S., 2000. Sensitivity of Cloud and Radiation Parameterizations to Changes in Vertical Resolution.

Tardif, R., 2007. The impact of vertical resolution in the explicit numerical forecasting of radiation fog: a case study. Pure Appl. Geophys. 164, 1221–1240.

Tie, X., Madronich, S., Li, G., Ying, Z., Zhang, R., Garcia, A.R., Lee-Taylor, J., Liu, Y., 2007. Characterizations of chemical oxidants in Mexico City: a regional chemical dynamical model (WRF-Chem) study. Atmos. Environ. 41, 1989–2008.

Tompkins, A.M., Emanuel, K.A., 2000. The vertical resolution sensitivity of simulated equilibrium temperature and water-vapour profiles. Q. J. R. Meteorol. Soc. 126, 1219–1238.

Wang, Z., Sha, W., Ueda, H., 2000. Numerical Modeling of Pollutant Transport and Chemistry during a High-ozone Event in Northern Taiwan.

Wang, Z., Li, J., Wang, Z., Yang, W., Tang, X., Ge, B., Yan, P., Zhu, L., Chen, X., Chen, H., Wand, W., Li, J., Liu, B., Wang, X., Wand, W., Zhao, Y., Lu, N., Su, D., 2013. Modeling study of regional severe hazes over mid-eastern China in January 2013 and its implications on pollution prevention and control. Sci. China Earth Sci. 57, 3–13.

Wang, J., Wang, S., Jiang, J., Ding, A., Zheng, M., Zhao, B., Wong, D.C., Zhou, W., Zheng, G., Wang, L., Pleim, J.E., Hao, J., 2014a. Impact of aerosol–meteorology interactions on fine particle pollution during China's severe haze episode in January 2013. Environ. Res. Lett. 9, 094002.

Wang, Y., Ying, Q., Hu, J., Zhang, H., 2014b. Spatial and temporal variations of six criteria air pollutants in 31 provincial capital cities in China during 2013-2014. Environ. Int. 73, 413–422.

Wang, H., Shi, G.Y., Zhang, X.Y., Gong, S.L., Tan, S.C., Chen, B., Che, H.Z., Li, T., 2015a. Mesoscale modelling study of the interactions between aerosols and PBL meteorology

during a haze episode in China Jing–Jin–Ji and its near surrounding region – Part 2: aerosols' radiative feedback effects. Atmos. Chem. Phys. 15, 3277–3287.
Wang, M., Cao, C., Li, G., Singh, R.P., 2015b. Analysis of a severe prolonged regional haze episode in the Yangtze River Delta, China. Atmos. Environ. 102, 112–121.
Wang, Z., Huang, X., Ding, A., 2018. Dome effect of black carbon and its key influencing factors: a one-dimensional modelling study. Atmos. Chem. Phys. 18, 2821–2834.
Wilcox, E.M., Thomas, R.M., Praveen, P.S., Pistone, K., Bender, F.A., Ramanathan, V., 2016. Black carbon solar absorption suppresses turbulence in the atmospheric boundary layer. Proc. Natl. Acad. Sci. U. S. A. 113, 11794–11799.
Xian, P., Reid, J.S., Hyer, E.J., Sampson, C.R., Rubin, J.I., Ades, M., Asencio, N., Basart, S., Benedetti, A., Bhattacharjee, P.S., Brooks, M.E., Colarco, P.R., da Silva, A.M., Eck, T.F., Guth, J., Jorba, O., Kouznetsov, R., Kipling, Z., Sofiev, M., Perez Garcia-Pando, C., Pradhan, Y., Tanaka, T., Wang, J., Westphal, D.L., Yumimoto, K., Zhang, J., 2019. Current state of the global operational aerosol multi-model ensemble: an update from the International Cooperative for Aerosol Prediction (ICAP). Q. J. R. Meteorol. Soc.
Xu, Z., Huang, X., Nie, W., Shen, Y., Zheng, L., Xie, Y., Wang, T., Ding, K., Liu, L., Zhou, D., Qi, X., Ding, A., 2018. Impact of biomass burning and vertical mixing of residual-layer aged plumes on ozone in the Yangtze River Delta, China: a tethered-balloon measurement and modeling study of a multiday ozone episode. J. Geophys. Res.: Atmosphere 123 (11), 711–786 803.
Yang, Y., Russell, L.M., Lou, S., Liao, H., Guo, J., Liu, Y., Singh, B., Ghan, S.J., 2017. Dust-wind interactions can intensify aerosol pollution over eastern China. Nat. Commun. 8, 15333.
Ye, X., Song, Y., Cai, X., Zhang, H., 2016. Study on the synoptic flow patterns and boundary layer process of the severe haze events over the North China Plain in January 2013. Atmos. Environ. 124, 129–145.
Yu, H., 2002. Radiative effects of aerosols on the evolution of the atmospheric boundary layer. J. Geophys. Res. 107.
Zaveri, R., Peters, K., 1999. Anew Lumped Structure Photochemical Mechanism for Long-Scale Applications.
Zaveri, R.A., Easter, R.C., Fast, J.D., Peters, L.K., 2008. Model for simulating aerosol interactions and chemistry (MOSAIC). J. Geophys. Res. 113.
Zhang, Q., 2015. A heavy haze episode in Shanghai in December of 2013: characteristics, origins and implications. Aerosol Air Qual. Res. 19, 1881–1893.
Zhang, D.-L., Wang, X., 2003. Dependence of Hurricane intensity and structures on vertical resolution and time-step size. Adv. Atmos. Sci. 20, 711.
Zhang, Y., Ding, A., Mao, H., Nie, W., Zhou, D., Liu, L., Huang, X., Fu, C., 2016. Impact of synoptic weather patterns and inter-decadal climate variability on air quality in the North China Plain during 1980–2013. Atmos. Environ. 124, 119–128.